Phase-field crystal modeling of equilibrium bcc-liquid interfaces

Kuo-An Wu* and Alain Karma

Department of Physics, Northeastern University, Boston, Massachusetts 02115, USA
(Received 25 June 2007; published 8 November 2007)

We investigate the equilibrium properties of bcc-liquid interfaces modeled with a continuum phase-field crystal (PFC) approach [K. R. Elder and M. Grant, Phys. Rev. E **70**, 051605 (2004)]. A multiscale analysis of the PFC model is carried out which exploits the fact that the amplitudes of crystal density waves decay slowly into the liquid in the physically relevant limit where the freezing transition is weakly first order. This analysis yields a set of coupled equations for these amplitudes that is similar to the set of equations derived from Ginzburg-Landau (GL) theory [K.-A. Wu *et al.*, Phys. Rev. B **73**, 094101 (2006)]. The two sets only differ in the details of higher order nonlinear couplings between different density waves, which is determined by the form of the nonlinearity assumed in the PFC model and by the ansatz that all polygons with the same number of sides have equal weight in GL theory. Despite these differences, for parameters (liquid structure factor and solid density wave amplitude) of Fe determined from molecular dynamics (MD) simulations, the PFC and GL amplitude equations yield very similar predictions for the overall magnitude and anisotropy of the interfacial free-energy and density wave profiles. These predictions are compared with MD simulations as well as numerical solutions of the PFC model.

PACS number(s): 64.70.Dv, 68.08.−p, 81.16.Rf, 81.30.Fb

I. INTRODUCTION

The phase-field method is by now well-developed to simulate the continuum scale evolution of interfaces outside of equilibrium with application to solidification[1] and other materials science problems.[2,3] The method rests on a coarse-graining procedure that smears out the discrete atomic nature of the interface. Hence, the phenomenological form of the free-energy functional used to construct a conventional phase-field model generally needs to be tailored to reproduce quantitatively atomistically determined interfacial properties.

An important property in a crystal growth context is the anisotropy of the excess free-energy of the crystal-melt interface that is a key parameter controlling dendritic evolution.[4–10] This anisotropy is traditionally incorporated phenomenologically into the phase-field model by letting the free-energy density depend on the direction normal to the interface, itself expressed in terms of the gradient of the phase-field.[11–13] Computationally efficient implementations of these models have been successfully applied to simulate dendritic evolution in materials with both atomically rough[7,8,10] and faceted[14] interfaces. The conventional phase-field approach, however, falls short in problems where crystalline defects have a profound influence on morphological evolution. For example, solidification twins can dramatically alter both eutectic[15,16] and dendritic[17] microstructures, and crystalline defects ultimately control grain coalescence and microstructural evolution during and after the late stages of solidification.[18]

Over the last few years, the phase-field crystal (PFC) method has emerged as an attractive computational approach to tackle this class of problems where atomic and continuum scales are tightly coupled.[19–23] This method is rooted in phenomenological continuum theories used to study equilibrium and nonequilibrium patterns with "crystal-like" ordering in diverse contexts. The models most closely related to the PFC model in their mathematical formulation have appeared in studies of phase separation in block copolymers[24] and Rayleigh-Bénard convection.[25,26]

Since the free-energy of the PFC model is a functional of the density of the material, the model can also be cast[21] in the framework of classical density functional theory of freezing.[27–33] PFC simulations have the main advantage of resolving the atomic-scale density wave structure of a poly-crystalline material and of describing the defect-mediated evolution of this structure on time scales orders of magnitude longer than molecular dynamics (MD) simulations.[19–23]

While the PFC method has been shown to describe qualitatively a wide range of phenomena,[19–23] its predictive capability in a crystal growth context remains largely unexplored. We investigate in this paper to what degree the PFC model can reproduce quantitatively some key equilibrium properties of the crystal-melt interface, in particular, the magnitude and anisotropy of the interfacial free-energy γ. Well-developed atomistic methods to calculate these properties[34–39] have been applied to both face-centered-cubic (fcc) (Refs. 38–42) and body-centered-cubic (bcc) systems.[41–44]

Our study is based on the PFC model that is a reformulation of the Swift-Hohenberg equation[25] with conserved dynamics introduced by Elder *et al.*[19,20] This model favors bcc crystal ordering in three dimensions. Our analysis of this model is closely related to previous studies of melting carried out in the framework of Ginzburg-Landau (GL) theory. The GL theory originally developed for bcc-liquid interfaces by Shih *et al.*[45] predates the PFC model and was recently revisited[44] in the light of recent results from MD simulations. This re-examination showed that GL theory yields predictions of γ and its anisotropy in reasonably good agreement with MD simulations for Fe, and the same MD results are used here to benchmark PFC model predictions.

GL theory is derived from classical density functional theory that expresses the free-energy of the system as a functional of its density distribution $n(\vec{r})$, as in the PFC model. Furthermore, it makes the strong assumption that $n(\vec{r})$ can be expanded as a sum

$$n(\vec{r}) = n_0\left(1 + \sum_i u_i(\vec{r})e^{i\vec{K}_i \cdot \vec{r}} + \cdots\right), \qquad (1)$$

of density waves corresponding to the principal reciprocal lattice vectors (where the index i spans the set of 12 $\{\vec{K}_{110}\}$ vectors of the reciprocal fcc lattice for bcc ordering). The amplitudes $u_i(\vec{r})$ of these density waves are the order parameters used to construct the GL free-energy. These amplitudes decay in the liquid at a rate that depends generally on the angle between $\vec{K}_i$ and the directional normal to the solid-liquid interface, which makes γ anisotropic. The fact that the anisotropy predicted by GL theory is in reasonably good agreement with MD simulations suggests that this directional dependence is a main determinant of anisotropy.[44]

Since the crystal density field of the PFC model is also dominated by the principal reciprocal lattice vectors, we expect this model to yield similar predictions of bcc-liquid interfacial properties as GL theory. Of course, the two theories are not identical since the contribution of higher order reciprocal lattice vectors of magnitude larger than $|\vec{K}_{110}|$, corresponding to "$\cdots$" in Eq. (1) is small but nonvanishing in the PFC model. Furthermore, the strength of the nonlinear coupling between different density waves is determined by the form of the free-energy functional in the PFC model, while it is determined in GL theory by using the simplifying assumption that all closed polygons composed of principal reciprocal lattice vectors with the same number of sides have equal weight.[44,45] Despite these differences, we find here that the PFC model and GL theory yield very similar predictions of bcc-liquid interfacial properties that are in reasonably good quantitative agreement with MD simulations.

To relate formally the PFC model and GL theory, we carry out a weakly-nonlinear multiscale analysis of the PFC model. This type of analysis, pioneered in the context of Rayleigh-Bénard convection,[46] has provided a fundamental understanding of the universal behavior of nonequilibrium patterns close to the onset of instability.[26] It has also been revived recently in the framework of the renormalization group to derive computationally efficient implementations of the PFC model.[47,48] In the pattern formation context where this analysis was first developed, the distance from the onset of instability can be characterized generally by a small parameter ϵ, e.g., in Rayleigh-Bénard convection $\epsilon \sim (R - R_c)/R_c$ where R is the Rayleigh number and R_c is its critical value corresponding to the onset of instability. Furthermore, close to onset ($\epsilon \ll 1$), spatially periodic patterns are generally slowly modulated in space. Considering the simplest case of a one-dimensional pattern for illustrative purposes, it is natural to write the field variables characterizing such a pattern in a form $\sim A(Z)e^{iq_0z}$+c.c., where $Z \sim \epsilon^{1/2}z$ is a slow space variable, q_0 is the wavenumber of the perfectly ordered pattern, and c.c. denotes the complex conjugate. The standard amplitude-equation approach consists of using a multiscale expansion to obtain an equation for the complex amplitude $A(Z)$ starting from the underlying equations governing the evolution of the pattern. The complex amplitude $A(Z) \equiv u(Z)e^{i\Phi(Z)}$ carries information about both the local real amplitude $u(Z)$ of the pattern and its local spatial

periodicity, or wavenumber $q(Z) \approx q_0 + \epsilon^{1/2}\partial_Z\Phi$. Similarly, a dependence of the amplitude on a slow time variable (omitted from the present discussion) can also be introduced to describe the slow temporal evolution of the pattern.

For solid-liquid equilibrium, the pattern of interest is the three-dimensional crystal density field that is spatially modulated along the coordinate z normal to the solid-liquid interface. However, there is no direct analog of a small parameter ϵ that can be made arbitrarily small by tuning some control parameter, such as the externally imposed temperature gradient in the example of Rayleigh-Bénard convection. In contrast, ϵ is uniquely determined by liquid structure factor properties when relating the PFC model to classical DFT. Thus ϵ has a fixed value for a given material. For systems with low entropy of melting and atomically rough interfaces, however, ϵ turns out to be small enough (~ 0.1 for Fe) for a multiscale analysis to be just about justified quantitatively. This smallness originates physically from the fact that density waves decay slowly in the liquid over several atomic layer spacings. This makes ϵ, which is proportional to the square of the ratio of the layer spacing and the interface width, much smaller than unity. For faceted interfaces, however, density waves decay abruptly in the liquid and this expansion would break down.

This paper is organized as follows. In Sec. II, we briefly summarize the equations of the PFC model and construct the phase-diagram corresponding to bcc-liquid coexistence. In Sec. III, we derive the amplitude equations that describe the equilibrium profiles of density waves in the interface region from the aforementioned multiscale expansion. The phases Φ of the complex amplitudes turn out to be constant in the interface region at dominant order in this expansion, such that the density field can be described by Eq. (1) with real order parameters that are the $u_i(\vec{r})$'s. This allows us to define the free-energy as a functional of these order parameters and to compare in Sec. IV the PFC amplitude equations to GL theory.[44] This comparison is used to fix uniquely the parameters of the bare PFC model in terms of liquid structure factor properties and the solid density wave amplitude derived from MD simulations. Differences in the nonlinear coupling between density waves in the PFC amplitude equations and GL theory are also highlighted in this section. In Sec. V, we compare quantitatively the predictions of γ for different crystal faces obtained using (i) the direct numerical solution of the PFC model, (ii) the amplitude equations derived from the PFC model, (iii) GL theory,[44] and (iv) MD simulations. Finally, concluding remarks are given in Sec. V.

II. PHASE-FIELD CRYSTAL MODEL

A. Basic equations and scaling

We consider the simplest PFC model defined by the free-energy functional[19,20]

$$F = \int d\vec{r}\left\{\frac{\phi}{2}[a + \lambda(q_0^2 + \nabla^2)^2]\phi + g\frac{\phi^4}{4}\right\}, \qquad (2)$$

which is a transposition to crystalline solids of the Swift-Hohenberg model of pattern formation.[25] The conserved or-

der parameter ϕ is a dimensionless measure of the crystal density field measured from some constant reference value. The relationship of ϕ to the physical density will be specified in the next section. The wavenumber q_0 sets the magnitude $|\vec{K}_i|$ of the principal reciprocal lattice vectors that correspond to the first peak of the liquid structure factor $S(K)$ at melting, and hence sets the scale of the ordered crystalline pattern $\sim q_0^{-1}$. The parameters a and λ determine the shape of the polynomial approximation of the liquid structure factor $S(K)$ in the PFC model. They were fixed in previous studies (Refs. 20 and 21) by matching the peak value of $S(K)$ and $S(0)$, which is related to the liquid phase compressibility, to values of the real structure factor. As shown in the next section, the parameters a and λ are determined here instead by matching the peak value of $S(K)$ and its width (determined by the second derivative of the direct correlation function at q_0) to the values determined by classical density function theory. This turns out to be important for modeling solid-liquid interfacial properties since the decay rate of density waves in the liquid is directly related to this width. The parameter g, in turn, is uniquely fixed by the amplitude of density waves in the solid.

To render the calculations less cumbersome, it is useful to rewrite the free-energy functional in dimensionless form by defining the parameter

$$\epsilon = -\frac{a}{\lambda q_0^4} \qquad (3)$$

and making the substitutions

$$q_0 \vec{r} \rightarrow \vec{r}, \qquad (4)$$

$$\sqrt{\frac{g}{\lambda q_0^4}}\phi \rightarrow \psi, \qquad (5)$$

$$\frac{g}{\lambda^2 q_0^5}F \rightarrow \mathcal{F}, \qquad (6)$$

where all the transformed quantities to the right of the arrows are dimensionless and

$$\mathcal{F} = \int d\vec{r} \left\{ \frac{\psi}{2}[-\epsilon + (\nabla^2 + 1)^2]\psi + \frac{1}{4}\psi^4 \right\}. \qquad (7)$$

In this study, we restrict our attention to equilibrium properties of the crystal melt interface. The condition that the chemical potential must be spatially uniform in equilibrium yields the equation

$$\mu_E = \frac{\delta \mathcal{F}}{\delta \psi} = -\epsilon\psi + (\nabla^2 + 1)^2\psi + \psi^3, \qquad (8)$$

which is the starting point of the present study. Although the dimensionless formulation of the PFC model is more convenient to carry out calculations, we shall later transform the results back into dimensional form in order to make contact with GL theory and determine the phase-field parameters that appear in Eq. (2).

B. Phase diagram

To construct the phase diagram, we calculate separately the free-energy density (free-energy per unit volume) as a function of the mean density $\bar{\psi}$ in solid, denoted by $f_s(\bar{\psi})$, and liquid $f_l(\bar{\psi})$ using Eq. (7). We then use the standard common tangent construction, which is equivalent to equating the chemical potentials and grand potentials of the two phases, to obtain the equilibrium values of $\bar{\psi}$ in the solid ($\bar{\psi}_s$) and liquid ($\bar{\psi}_l$).

Since the density is constant in the liquid, f_l is obtained directly from Eq. (7)

$$f_l = -(\epsilon - 1)\frac{\bar{\psi}^2}{2} + \frac{\bar{\psi}^4}{4}. \qquad (9)$$

Furthermore, since ϵ turns out to be a small parameter for spatially diffuse atomically rough interfaces, the solid free-energy density can be well approximated by only considering the contribution of the principal reciprocal lattice vectors. Accordingly, the crystal density field can be written in the form analogous to Eq. (1)

$$\psi(\vec{r}) \approx \bar{\psi} + \sum_i A_i e^{i\vec{K}_i \cdot \vec{r}} \approx \bar{\psi} + 4A_s(\cos qx \cos qy$$
$$+ \cos qx \cos qz + \cos qy \cos qz), \qquad (10)$$

where we have used the fact that all density waves have the same amplitude ($|A_i| = A_s$) and all principal reciprocal lattice vectors of the bcc structure have the same magnitude ($|\vec{K}_{110}| = |\vec{K}_{1-10}| = \cdots = \sqrt{2}q$). The parameters A_s and q are solved by substituting Eq. (10) into Eq. (7) and minimizing the resulting free-energy with respect to A_s and q, which yields

$$A_s = -\frac{2}{15}\bar{\psi} + \frac{1}{15}\sqrt{5\epsilon - 11\bar{\psi}^2} \qquad (11)$$

and $q = 1/\sqrt{2}$, together with the expression for the solid free-energy density (for $q = 1/\sqrt{2}$)

$$f_s = -(\epsilon - 1)\frac{\bar{\psi}^2}{2} + \frac{\bar{\psi}^4}{4} - 6\epsilon A_s^2 + 18\bar{\psi}^2 A_s^2 + 48\bar{\psi}A_s^3 + 135A_s^4. \qquad (12)$$

Applying the common tangent construction, which is detailed below in the small ϵ limit, yields the bcc-liquid coexistence region in the phase diagram of Fig. 1. Also shown are the other two-dimensional crystal structures (hexagonal and stripe phases) determined in previous studies using the same approximation where the crystal density field is a sum of density waves corresponding to the set of principal reciprocal lattice vectors.[19,20]

III. DERIVATION OF THE AMPLITUDE EQUATIONS

A. Small ϵ analysis of the phase diagram

For small ϵ, we can seek a perturbative solution of the crystal density field ψ in powers of $\epsilon^{1/2}$ as suggested by the scaling of various terms in Eq. (8)
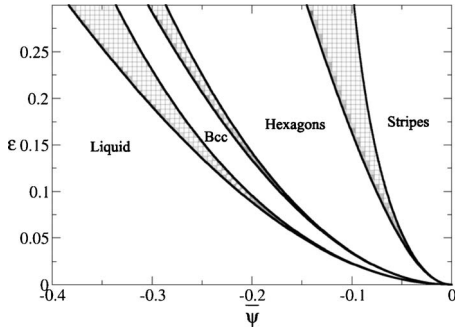
FIG. 1. Phase diagram of the PFC model obtained under the approximation that the crystal density field is as a sum of density waves corresponding to the set of principal reciprocal lattice vectors for a given crystal structure.

$$\psi(\vec{r}) = \psi_0(\vec{r})\epsilon^{1/2} + \psi_1(\vec{r})\epsilon + \psi_2(\vec{r})\epsilon^{3/2} + \cdots \quad (13)$$

and expand accordingly the average densities

$$\overline{\psi_s} = \psi_{s0}\epsilon^{1/2} + \psi_{s1}\epsilon + \psi_{s2}\epsilon^{3/2} + \cdots \quad (14)$$

and

$$\overline{\psi_l} = \psi_{l0}\epsilon^{1/2} + \psi_{l1}\epsilon + \psi_{l2}\epsilon^{3/2} + \cdots \quad (15)$$

in the solid and liquid, respectively. Substituting these relations into the expressions for f_s and f_l, using the conditions of equality of the chemical potentials of the two phases $f_s'(\overline{\psi_s}) = f_l'(\overline{\psi_l}) = \mu_E$ and equality of the grand potentials $f_s(\overline{\psi_s}) - \mu_E\overline{\psi_s} = f_l(\overline{\psi_l}) - \mu_E\overline{\psi_l}$, and collecting powers of ϵ, we obtain

$$\psi_{s0} = \psi_{l0} \equiv \psi_c = -\sqrt{\frac{45}{103}} \quad (16)$$

and

$$\psi_{s1} = \psi_{l1} = 0. \quad (17)$$

This shows that, in the small ϵ limit, the PFC model exhibits a weak first-order freezing transition where the size of the solid-liquid coexistence region $\Delta\overline{\psi} = \overline{\psi_s} - \overline{\psi_l} \approx (\psi_{s2} - \psi_{l2})\epsilon^{3/2}$ is much smaller than the mean value of the density $\sim \epsilon^{1/2}$. These scalings imply that the mean density difference between the two phases only gives a small higher order correction to the density wave profiles through the interface and γ in the small ϵ limit.

B. Multiscale expansion

Using Eqs. (14) and (15) to evaluate the small ϵ limit of the chemical potential $\mu_E = f_l'(\overline{\psi_l}) = f_s'(\overline{\psi_s})$, the equilibrium equation of the density field (8) becomes

$$-\epsilon\psi + (\nabla^2 + 1)^2\psi + \psi^3 = \psi_c\epsilon^{1/2} + (\psi_{l2} - \psi_c + \psi_c^3)\epsilon^{3/2} + \cdots. \quad (18)$$

The derivation of the amplitude equation exploits the separation of scale between the width of the spatially diffuse interface and the interatomic layer spacing in the small ϵ

limit. This separation of scale allows us to assume that the envelope of density waves depends on a slow spatial variable $Z \equiv \epsilon^{1/2}z$ [i.e., $\psi_0(\vec{r}) = \psi_c + \Sigma A_i^0(Z)e^{i\vec{K}_i \cdot \vec{r}}$, and so on for higher order terms], where z denotes the coordinate along the direction normal to the solid-liquid interface. The multiscale expansion rests on treating the slow variable Z and the fast variable z as independent variables. Thus the spatial derivative along z transforms with the chain rule $\partial_z \to \partial_z + \epsilon^{1/2}\partial_Z$, and the differential operator $L^2 \equiv (\nabla^2 + 1)^2$ in Eq. (18) becomes

$$L^2 \to L^2 + 4\epsilon^{1/2}L\partial_z\partial_Z + 2\epsilon(L + 2\partial_z^2)\partial_Z^2, \quad (19)$$

where the differential operator L on the right-hand-side only acts on the fast spatial variable z.

Next, we substitute the small ϵ expansion of the density field (13) into the equilibrium equation (18) with the above transformation of the linear operator. Collecting terms with the same power ϵ, we find at the order $\epsilon^{1/2}$

$$L^2\psi_0 = \psi_c, \quad (20)$$

which has the solution

$$\psi_0 = \sum_i A_i^0(Z)e^{i\vec{K}_i \cdot \vec{r}} + \psi_c, \quad (21)$$

where $|\vec{K}_i| = 1$ in our scaled units. At order ϵ, we obtain

$$L^2\psi_1 = 0, \quad (22)$$

which has the solution

$$\psi_1 = \sum_i A_i^1(Z)e^{i\vec{K}_i \cdot \vec{r}}, \quad (23)$$

and collecting the terms at order $\epsilon^{3/2}$ yields

$$L^2\psi_2 + (4\partial_z^2\partial_Z^2 - 1)\psi_0 + \psi_0^3 = \psi_{l2} - \psi_c + \psi_c^3. \quad (24)$$

The amplitude equations are obtained from the condition for the existence of a solution of the above equation without needing to compute ψ_2 explicitly. Since $L^2\psi_2$ gives a vanishing contribution for all density waves associated with the set $\{\vec{K}_i\}$ of twelve principal reciprocal lattice vectors of magnitude unity [i.e., $L^2e^{i\vec{K}\cdot\vec{r}} = (-|K|^2 + 1)^2e^{i\vec{K}\cdot\vec{r}} = 0$ if $|\vec{K}|^2 = 1$], all remaining terms $\sim e^{i\vec{K}_i\cdot\vec{r}}$ must balance each other in order for a solution of Eq. (24) to exist (i.e., secular terms must cancel out each other). For example, the condition that the coefficients of $e^{i\vec{K}_{011}\cdot\vec{r}}$ balance each other yields

$$[4(\hat{K}_{011} \cdot \hat{n})^2\partial_Z^2 + 3\psi_c^2 - 1]A_{011}^0 + (3|A_{011}^0|^2 + 6|A_{110}^0|^2$$
$$+ 6|A_{1\bar{1}0}^0|^2 + 6|A_{101}^0|^2 + 6|A_{10\bar{1}}^0|^2 + 6|A_{01\bar{1}}^0|^2)A_{011}^0$$
$$+ 6A_{01\bar{1}}^0 A_{10\bar{1}}^{0*} A_{101}^0 + 6A_{01\bar{1}}^{0*} A_{110}^0 A_{1\bar{1}0}^{0*} + 6A_{101}^0 A_{1\bar{1}0}^{0*}\psi_c$$
$$+ 6A_{110}^0 A_{10\bar{1}}^{0*}\psi_c = 0, \quad (25)$$

where everywhere in this paper $\hat{z} = \hat{n}$ corresponds to the direction normal of the interface that generally differs from the crystal axes except for {100} crystal faces. This solvability condition must be satisfied independently for each $\vec{K}_i$. This

yields a set of twelve coupled amplitude equations (i.e., eleven additional equations to the one above) that are straightforward to obtain and we do not list them all here for brevity of presentation. These equations can also be obtained directly from the free-energy expressed as a functional of the amplitudes $A_i^0(Z)$ as described in the next subsection.

The amplitude profiles are governed by these twelve coupled nonlinear amplitude equations. These equations can be reduced to a simple set of equations by considering the symmetry of reciprocal lattice vectors. For {100} crystal faces, these twelve amplitudes can be separated into two subsets with the same value of $(\vec{K}_i \cdot \hat{n})^2$ equal to 1/2 and 0, respectively. Therefore, the amplitude equations are reduced to only two coupled equations and can be solved numerically. Similarly, we have two subsets of amplitudes for {111} crystal faces and three subsets of amplitudes for {110} crystal faces, which results in two and three coupled amplitude equations, respectively.

As in GL theory,[44] the γ anisotropy originates from the fact that the coefficients of the second derivative terms in the amplitude equations depend on $(\hat{K}_i \cdot \hat{n})$ and hence on the orientation of the crystal face with respect to a fixed set of crystal axes. Furthermore, as mentioned in the introduction, since the amplitudes are complex, the spatial variation of the phase can cause the local wave vector to change through the solid-liquid interface by an amount proportional to the gradient of this phase. To determine this variation, we substitute

$$A_i^0(Z) = |A_i^0(Z)|e^{i\Phi_i(Z)} \qquad (26)$$

into the amplitude equations. We obtain that $\Phi_i(Z)=0$ for the principal reciprocal lattice vectors that are orthogonal to the interface normal and

$$\frac{1}{|A_i^0(Z)|}\partial_Z[|A_i^0(Z)|^2\Phi_i(Z)] = 0 \qquad (27)$$

for the other reciprocal lattice vectors. The above equation implies that

$$|A_i^0(Z)|^2\partial_Z\Phi_i(Z) = C_0, \qquad (28)$$

where C_0 is a constant. Since the amplitudes must vanish in liquid, the divergence of $d\Phi_i/dZ$ can be avoided only if $C_0 = 0$. Therefore, the wave vectors $\vec{K}_i$'s are constant through the solid-liquid interface in the small ϵ limit.

C. Free-energy functional

It is useful to express the free-energy of the solid-liquid system as a functional of the density wave amplitudes A_i^0. For this, we define $\Delta\mathcal{F}$ to be the free-energy measured from its constant value in the liquid. Since the amplitudes are non-conserved order parameters, the equilibrium state simply corresponds to a minimum of this free-energy without extra constraint. This implies that $\Delta\mathcal{F}$ should be chosen such that the amplitude equations are recovered variationally from this free-energy. Namely, the equation for a given A_i^0 derived in the last subsection should be equivalent to

$$\frac{\delta\Delta\mathcal{F}}{\delta A_i^{0*}} = 0, \qquad (29)$$

up to a multiplicative constant. This constant can be determined by matching the limiting value of $\Delta\mathcal{F}/V$ on the solid-side, where all the amplitudes are constant ($A_i^0 = \epsilon^{-1/2}A_s$ for all i) to the difference of free-energy densities between the two phases $f_s - f_l$, where f_s and f_l are given by Eqs. (9) and (12) and V is the volume. This yields the free-energy functional

$$\Delta\mathcal{F} = \epsilon^{3/2}\Omega \int dZ\left[\sum_i 2(\hat{K}_i \cdot \hat{n})^2\left|\frac{dA_i^0}{dZ}\right|^2 + f(A_i^0)\right], \quad (30)$$

where $\Omega \equiv \int dxdy$ is the interface area and

$$
\begin{aligned}
f(A_i^0) = &\frac{1}{2}\sum_i (3\psi_c^2 - 1)|A_i^0|^2 + \frac{3}{4}\sum_i\sum_{j\neq i}|A_i^0|^2|A_j^0|^2 \\
&+ 6A_{110}^{0*}A_{1\bar{1}0}^{0*}A_{101}^0A_{10\bar{1}}^0 + 6A_{110}^0A_{1\bar{1}0}^0A_{101}^{0*}A_{10\bar{1}}^{0*} \\
&+ 6A_{1\bar{1}0}^0A_{011}^0A_{01\bar{1}}^0A_{110}^{0*} + 6A_{1\bar{1}0}^{0*}A_{011}^{0*}A_{01\bar{1}}^{0*}A_{110}^0 \\
&+ 6A_{01\bar{1}}^0A_{10\bar{1}}^{0*}A_{101}^0A_{011}^{0*} + 6A_{01\bar{1}}^{0*}A_{10\bar{1}}^0A_{101}^{0*}A_{011}^0 \\
&+ 6\psi_cA_{011}^{0*}A_{101}^0A_{1\bar{1}0}^{0*} + 6\psi_cA_{011}^0A_{101}^{0*}A_{1\bar{1}0}^0 \\
&+ 6\psi_cA_{011}^{0*}A_{110}^0A_{10\bar{1}}^{0*} + 6\psi_cA_{011}^0A_{110}^{0*}A_{10\bar{1}}^0 \\
&+ 6\psi_cA_{01\bar{1}}^{0*}A_{110}^0A_{101}^{0*} + 6\psi_cA_{01\bar{1}}^0A_{110}^{0*}A_{101}^0 \\
&+ 6\psi_cA_{011}^{0*}A_{10\bar{1}}^0A_{1\bar{1}0}^{0*} + 6\psi_cA_{011}^0A_{10\bar{1}}^{0*}A_{1\bar{1}0}^0.
\end{aligned} \qquad (31)
$$

It is simple to check that by applying Eq. (29) to the above functional for $A_i^0 = A_{011}$ we obtain the same amplitude equation as Eq. (25) and similarly for the other principal reciprocal lattice vectors. Finally, Eq. (6) implies that the dimensional free-energy functional derived from the amplitude equations (AE) is given by

$$\Delta F_{\text{AE}} = \frac{\lambda^2 q_0^5}{g}\Delta\mathcal{F}. \qquad (32)$$

IV. COMPARISON OF AMPLITUDE EQUATIONS AND GINZBURG-LANDAU THEORY

In this section, we compare the free-energy functional derived from the PFC amplitude equations to GL theory.[44] This comparison sheds light on the relation between this theory and the PFC model and uniquely fixes the parameters of the latter in terms of physical quantities that can be extracted from MD simulations.

A. Ginzburg-Landau theory

The free-energy functional of GL theory is expressed in terms of the amplitude u_i of density waves defined by Eq. (1). We write this functional here for convenience using the same notation as in Ref. 44 with the direction normal to the solid-liquid interface parallel to the z axis

$$\Delta F_{GL} = \frac{n_0 k_B T \Omega}{2} \left(\int dz a_2 \sum_{i,j} c_{ij} u_i u_j \delta_{0,\vec{K}_i + \vec{K}_j} \right.$$

$$- a_3 \sum_{i,j,k} c_{ijk} u_i u_j u_k \delta_{0,\vec{K}_i + \vec{K}_j + \vec{K}_k}$$

$$\left. + a_4 \sum_{i,j,k,l} c_{ijkl} u_i u_j u_k u_l \delta_{0,\vec{K}_i + \vec{K}_j + \vec{K}_k + \vec{K}_l} + b \sum_i c_i \left| \frac{du_i}{dz} \right|^2 \right), \tag{33}$$

where $\delta_{m,n}$ is the Kronecker delta that equals 0 or 1 for $m \neq n$ or $m = n$, respectively. The latter enforces that only combinations of principal reciprocal lattice vectors that form closed polygons $\vec{K}_i + \vec{K}_j + \cdots = 0$ contribute to the free-energy functional. The multiplicative factors a_i and b are introduced since it is convenient to normalize the sums of the c's to unity (i.e., $\Sigma_i c_i = 1$, $\Sigma_{i,j} c_{ij} \delta_{0,\vec{K}_i + \vec{K}_j} = 1$, etc.).

The coefficients of quadratic nonlinearities of the GL free-energy were determined in Ref. 44 by relating ΔF_{GL} to the free-energy functional that describes small density fluctuations of an inhomogeneous liquid in the simplest formulation of DFT [Eq. (3) in Ref. 44]. In particular, the latter can be reduced to the form[28]

$$\Delta F_{DFT} \approx \frac{n_0 k_B T \Omega}{2} \int dz \left[\sum_{i,j} \frac{1}{S(|\vec{K}_i|)} u_i u_j \delta_{0,\vec{K}_i + \vec{K}_j} \right.$$

$$\left. - \sum_i \frac{1}{2} C''(|\vec{K}_i|)(\hat{K}_i \cdot \hat{n})^2 \left| \frac{du_i}{dz} \right|^2 \right] \tag{34}$$

by assuming that the density wave amplitudes vary slowly through the interface region and are essentially constant on the scale of the interatomic layer spacing. The small ϵ multiscale expansion of the last section is an alternative procedure to derive the form of Eq. (34) that formalizes this assumption. Here $C(K)$ is the Fourier transform of the direct correlation function $C(|\vec{r}|)$

$$C(K) = n_0 \int d\vec{r} C(|\vec{r}|) e^{-i\vec{K} \cdot \vec{r}}, \tag{35}$$

and $S(K) = [1 - C(K)]^{-1}$ is the liquid structure factor.

Equating ΔF_{GL} and ΔF_{DFT} at quadratic order in the nonlinearities and using the normalization that the sums of c_i's and c_{ij}'s equal unity, we obtain

$$c_{ij} = 1/12, \tag{36}$$

$$c_i = \frac{1}{4}(\hat{K} \cdot \hat{n})^2, \tag{37}$$

$$a_2 = \frac{12}{S(K_{max})}, \tag{38}$$

$$b = -2C''(K_{max}), \tag{39}$$

where the magnitude $|\vec{K}_i| = q_0$ of the principal reciprocal lattice vectors can be set equal to the K value corresponding to the first peak of the structure factor K_{max} under the assump-

tion that the wave vectors are constant in the interface region. This assumption was formally justified in the derivation of the amplitude equations in Sec. III B by showing that the phase Φ of the complex amplitudes is constant in the interface region at leading order in the small ϵ expansion. The reader is referred to Ref. 44 for the determination of the cubic and quartic nonlinearities in the GL theory, which shall be briefly reviewed below.

B. Determination of phase-field crystal model parameters

We are now in a position to compare the free-energy functionals derived from the amplitude equations and GL theory and to relate the parameters of the PFC model to physical quantities. For this, we note that ΔF_{AE} has the same form as ΔF_{GL} because the density wave amplitudes A_i^0's and u_i's proportionally related. The proportionality constant is readily obtained by combining Eq. (5) and Eq. (13), which yields

$$n_0 u_i = \sqrt{\frac{\lambda q_0^4}{g}} \epsilon^{1/2} A_i^0. \tag{40}$$

Furthermore, Eq. (29) used to construct ΔF_{AE} is equivalent to the constraint that only combinations of principal reciprocal lattice vectors that form closed polygons contribute to the free-energy functional as shown explicitly in Eq. (31).

Next, using Eq. (40) and equating ΔF_{AE}, defined by Eqs. (30) and (32), and ΔF_{GL} defined by Eq. (33), we obtain the relations

$$a_2 = \frac{12 n_0 a (1 - 3\psi_c^2)}{k_B T} = \frac{12}{S(K_{max})}, \tag{41}$$

$$b = \frac{16 n_0 \lambda q_0^2}{k_B T} = -2C''(K_{max}), \tag{42}$$

where we made use of Eqs. (38) and (39) to write the second equalities and $\psi_c = -\sqrt{45/103}$ as shown earlier. Equations (41) and (42) uniquely relate the parameters a and λ of the PFC model to peak properties of the liquid structure factor that can be computed from MD simulations or measured experimentally. They also fix the value of ϵ related to a and λ by Eq. (3)

$$\epsilon = \frac{8}{(1 - 3\psi_c^2)q_0^2 S(K_{max})C''(K_{max})}. \tag{43}$$

The only left unknown parameter g of the PFC model can be obtained by applying Eq. (40) in the solid where all the density wave amplitudes have equal magnitude. Substituting into Eq. (40) $u_i = u_s$ and the solid value of the amplitudes

$$A_i^0 = \epsilon^{-1/2} A_s = -\frac{2}{15}\psi_c + \frac{1}{15}\sqrt{5 - 11\psi_c^2}, \tag{44}$$

which follows from Eq. (11) or Eq. (25), we obtain the relation

$$g = \lambda q_0^4 \left(-\frac{2}{15}\psi_c + \frac{1}{15}\sqrt{5 - 11\psi_c^2} \right)^2 \Big/ (n_0^2 u_s^2). \tag{45}$$

This relation fixes g in terms of the other parameters and u_s, which can be extracted directly from MD simulations[44] or

related to the latent heat of melting and the temperature dependence of $S(K_{max})$.[44,45]

C. Coefficients of quartic nonlinearities

The free-energy functionals derived from the PFC amplitude equations and GL theory only differ in the values of the coefficients of higher order nonlinearities. As we shall see in the next section, these differences turn out to be unimportant because the amplitude equations and GL theory yield essentially identical predictions of γ and its anisotropy. However, they deserve brief mention. In GL theory, the coefficients a_3 and a_4 are determined from the two equilibrium conditions that (i) the solid and liquid phases must have equal free-energies at melting $\Delta F_{GL}|_{u_i=u_s}=0$, and (ii) the equilibrium state of the solid is a minimum of free-energy $\partial \Delta F_{GL}/\partial u_i|_{u_i=u_s}=0$. These two conditions yield the relations[44,45]

$$a_3 = 2a_2/u_s \qquad (46)$$

and

$$a_4 = a_2/u_s^2. \qquad (47)$$

The amplitude-equation free-energy functional ΔF_{AE} satisfies automatically the above two equilibrium conditions by construction. Thus, it only differs from ΔF_{GL} in the calculation of the other coefficients of the cubic and quartic terms c_{ijk} and c_{ijkl}. In GL theory, these coefficients by the ansatz that all closed polygons of $\vec{K}_i$'s with the same number of sides have the same weight, which yields $c_{ijk}=1/8$ and $c_{ijkl}=1/27$.[44]

In contrast, in the PFC amplitude equations, these coefficients are uniquely determined by the choice of the nonlinear terms in the original PFC free-energy functional. For the simplest choice of nonlinearity $\sim \phi^4$ considered here, the amplitude equation derivation yielded the same coefficients of cubic terms as GL theory but different coefficients of quartic terms. Comparing Eq. (33) with Eqs. (30) and (32), we obtain that, in the expression for ΔF_{AE}, $c_{ijkl}=1/90$ for two-sided polygons that contain only two wave vectors $\vec{K}_i$ and $-\vec{K}_i$, and $c_{ijkl}=4/90$ for the rest of the quartic terms.

To make these differences explicit, we consider the {110} crystal faces. The set of 12 principal reciprocal lattice vectors corresponding to $\langle 110 \rangle$ direction can be separated into three subsets with the same value of $(\hat{K}_i \cdot \hat{n})^2$: subset I with eight vectors ([011], [0$\bar{1}$1], [01$\bar{1}$], [101], [$\bar{1}$01], [10$\bar{1}$], [0$\bar{1}\bar{1}$], [$\bar{1}$0$\bar{1}$]) and $(\hat{K}_i \cdot \hat{n})^2=1/4$, subset II with two vectors ([110], [$\bar{1}\bar{1}$0]) and $(\hat{K}_i \cdot \hat{n})^2=1$, and subset III with two vectors ([$\bar{1}$10], [1$\bar{1}$0]) and $(\hat{K}_i \cdot \hat{n})^2=0$. Density waves in a given subset have the same amplitude denoted here by u, v, and w for subsets I, II, and III, respectively. Then for {110} crystal faces, Eqs. (30) and (32) reduce to

$$\Delta F_{AE} = \frac{n_0 k_B T \Omega}{2} \int dz \left[a_2 \left(\frac{2}{3}u^2 + \frac{1}{6}v^2 + \frac{1}{6}w^2 \right) - a_3 \left(\frac{1}{2}u^2 v \right. \right.$$
$$\left. + \frac{1}{2}u^2 w \right) + a_4 \left(\frac{36}{90}u^4 + \frac{1}{90}v^4 + \frac{1}{90}w^4 + \frac{16}{90}u^2 v^2 \right.$$
$$+ \frac{16}{90}u^2 w^2 + \frac{4}{90}w^2 v^2 + \frac{16}{90}u^2 vw \right) - C''(|\vec{K}_{110}|) \left| \frac{du}{dz} \right|^2$$
$$\left. - C''(|\vec{K}_{110}|) \left| \frac{dv}{dz} \right|^2 \right], \qquad (48)$$

and differ from the corresponding expression obtained from GL theory

$$\Delta F_{GL} = \frac{n_0 k_B T \Omega}{2} \int dz \left[a_2 \left(\frac{2}{3}u^2 + \frac{1}{6}v^2 + \frac{1}{6}w^2 \right) - a_3 \left(\frac{1}{2}u^2 v \right. \right.$$
$$\left. + \frac{1}{2}u^2 w \right) + a_4 \left(\frac{12}{27}u^4 + \frac{1}{27}v^4 + \frac{1}{27}w^4 + \frac{4}{27}u^2 v^2 \right.$$
$$+ \frac{4}{27}u^2 w^2 + \frac{1}{27}w^2 v^2 + \frac{4}{27}u^2 vw \right) - C''(|\vec{K}_{110}|) \left| \frac{du}{dz} \right|^2$$
$$\left. - C''(|\vec{K}_{110}|) \left| \frac{dv}{dz} \right|^2 \right]. \qquad (49)$$

V. COMPARISON OF CONTINUUM THEORIES AND MOLECULAR DYNAMICS SIMULATIONS

In Ref. 44, the predictions of GL theory were compared to MD simulations of Fe with interatomic potentials developed by Mendelev, Han, Srolovitz, Ackland, Sun, and Asta [MH(SA)^2] based on the embedded atom method.[49] In this section, we extend this comparison to include the predictions of both the PFC model, with the free-energy functional defined by Eq. (2) and the amplitude equations derived from this model with the free-energy functional defined by Eqs. (30) and (32). We use the same MD simulation results for the present comparison. Details of the MD simulations and of the method to extract the density wave profiles from these simulations are given in Ref. 44 and need not be repeated here.

The input parameters for the different continuum theories are computed from the MD simulations in order to make the comparison with these simulations as quantitative and precise as possible. These include the parameters related to peak properties of the liquid structure factor $K_{max}=q_0=2.985$ Å^{-1}, $1/S(K_{max})=0.332$, $C''(K_{max})=-10.40$ Å^2, and the amplitude of density waves corresponding to the principal reciprocal lattice vectors in the solid $u_s=0.72$. These input parameters fix the various coefficients of the continuum theories derived in the last section, which are listed in Table I.

The calculation of density wave profiles and γ values for the PFC amplitude equations, Eqs. (30) and (32), proceeds in the same way as for GL theory.[44] For example, for the case of the {110} crystal faces elaborated in Sec. IV C, the density wave profiles were calculated by minimizing ΔF_{AE} given by Eq. (48) with respect to the order parameters u, v, and w, and by solving numerically the resulting set of coupled ordinary differential equations with the boundary condition $u=v=w$

TABLE I. Values of input parameters from MD simulations with interatomic EAM potential for Fe from MH(SA) (Refs. 2 and 49) and resulting coefficients used in GL theory, the PFC model, and the amplitude equations derived from this model.

	n_0 (Å^{-3})	a_2	b (Å^2)	u_s	q_0 (Å^{-1})	a (eV Å^3)	λ (eV Å^7)	g (eV Å^9)	ϵ
MD [MH(SA)^2] (Ref. 41)	0.0765	3.99	20.81	0.72	2.985	−2.136	0.291	9.705	0.0923

$=u_s$ in solid and $u=v=w=0$ in liquid. The value of $\gamma_{110}=\Delta F_{AE}/\Omega$ was then computed by integration of Eq. (48) with these profiles. The same procedure was repeated for the {100} and {111} crystal faces, with different set of order parameters for each crystal face.

To compute γ in PFC simulations, we first relax the density field ψ to a minimum of the free-energy functional $\mathcal{F} \equiv \int d\vec{r} f$, where the free-energy density f is the integrand of Eq. (7), using a simple diffusive dynamics. We then compute γ in dimensional units using the relation

$$\gamma = \Omega^{-1}\frac{\lambda^2 q_0^5}{g} \int d\vec{r}\left[f - \left(f_s\frac{\psi - \bar{\psi}_l}{\bar{\psi}_s - \bar{\psi}_l} - f_l\frac{\psi - \bar{\psi}_s}{\bar{\psi}_s - \bar{\psi}_l}\right)\right], \quad (50)$$

where $\bar{\psi}_s$ ($\bar{\psi}_l$) and f_s (f_l) are the mean values of ψ and the free-energy density in solid (liquid), respectively, and $\Omega = \int dxdy$ is the interface area. Although ϵ is small, these values need to be computed numerically (i.e., by calculating the solid free-energy density from the numerical solution of the PFC model rather than using the weakly nonlinear approximations derived in Sec. II) in order to obtain an accurate computation of γ.

The predictions of the different continuum theories are compared to MD simulations in Table II. Interestingly, despite the differences in quartic coefficients described in Sec. IV C, the PFC amplitude equations and GL theory give essentially identical predictions. The density wave profiles predicted by the two theories are almost indistinguishable on the scale of Fig. 2. Furthermore, the predicted γ values by the different continuum theories for a given crystal face do not differ by more than a few tenth of a percent. Both theories predict a weak fourfold anisotropy $\epsilon_4 \equiv (\gamma_{100}-\gamma_{110})/(\gamma_{100}+\gamma_{110})$ close to one percent consistent with the results of MD simulations with the MH(SA)^2 EAM potential[49] for Fe.

The PFC simulations predict essentially the same anisotropy value but about 10% larger γ values that are in closer

agreement with MD simulation results. The larger γ values can be attributed to larger $|\vec{K}|$ modes and to the variation of the mean density in the interface region, both of which are neglected in the weakly-nonlinear amplitude equations and GL theory.

The anisotropy parameter ϵ_4 defined in terms of γ_{100} and γ_{110} has been traditionally used to quantify the magnitude of anisotropy in dendrite growth theory.[4–8] As seen in Table II, this parameter is reasonably well predicted by the PFC simulations and amplitude equations or GL theory. Over the past few years, however, numerous MD simulation studies have consistently found that at least two anisotropy parameters ϵ_1 and ϵ_2 are necessary to represent the entire γ-plot of fcc-liquid and bcc-liquid interfaces in diverse systems.[9] These parameters are defined by the expansion of γ in terms of cubic harmonics (i.e., combination of spherical harmonics with cubic symmetry) that has the form

$$\gamma(\hat{n}) = \gamma_0\left[1 + \epsilon_1\left(\sum_{i=1}^{3} n_i^4 - \frac{3}{5}\right)\right.$$
$$\left. + \epsilon_2\left(3\sum_{i=1}^{3} n_i^4 + 66 n_1^2 n_2^2 n_3^2 - \frac{17}{7}\right)\right], \quad (51)$$

where the n_i's are the coordinates of the direction normal to the interface ($\hat{n}$) in a set of cartesian coordinates parallel to the crystal axes. Values of γ for the the three independent crystal faces listed in Table II uniquely fix γ_0, ϵ_1, and ϵ_2. While a positive ϵ_1 favors dendrite growth along the set of six $\langle 100\rangle$ directions, a negative ϵ_2 favors growth along the set of twelve $\langle 110\rangle$ directions. A recent phase-field simulation study has revealed the existence of hyperbranched dendrite morphologies with a basic set of twenty four growth directions between $\langle 100\rangle$ and $\langle 110\rangle$ over some region of the (ϵ_1, ϵ_2) parameter space, where $\epsilon_1 > 0$ and $\epsilon_2 < 0$ favor different growth directions.[10]

TABLE II. Comparison of γ values for different crystal faces (in erg/cm^2) and anisotropy parameters including $\epsilon_4 \equiv (\gamma_{100}-\gamma_{110})/(\gamma_{100}+\gamma_{110})$ in percent and ϵ_1 and ϵ_2 values (see text), predicted by MD simulations, and by various continuum theories (PFC simulations, PFC amplitude equations, and GL theory) with the input parameters of Table I from MD simulations.

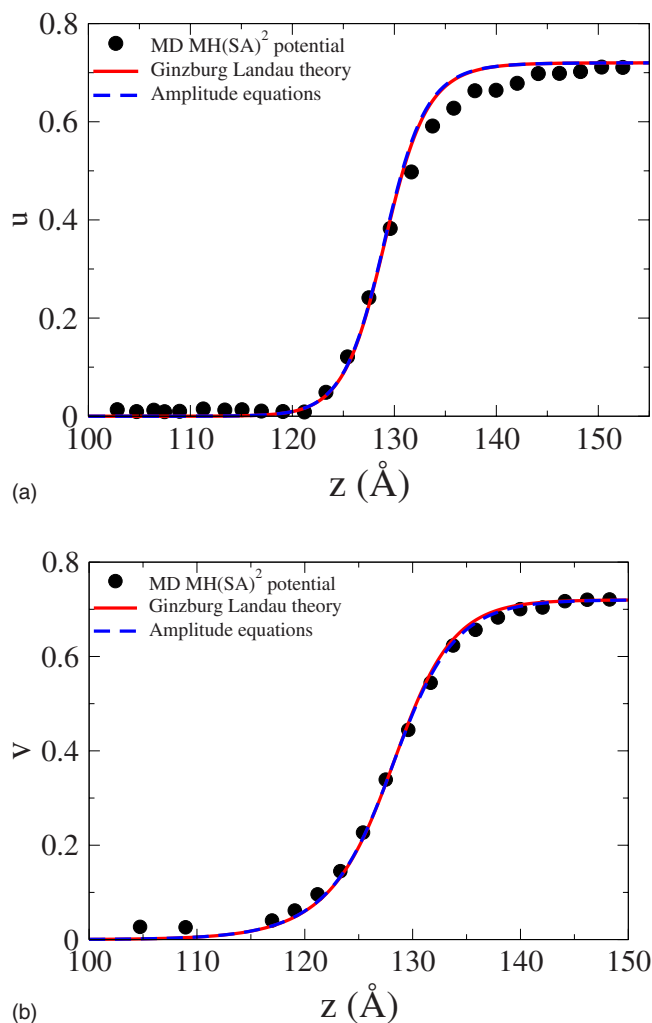|	100	110	111	$\epsilon_4(\%)$	ϵ_1	ϵ_2
MD [MH(SA)^2] (Ref. 41)	177.0 (10.8)	173.5 (10.6)	173.4 (10.6)	1.0(0.6)	0.033	0.0025
PFC simulation	160.47	156.83	152.00	1.15	0.075	−0.0094
Amplitude equations	144.14	140.67	135.76	1.22	0.082	−0.0110
GL theory (Ref. 44)	144.26	141.35	137.57	1.02	0.066	−0.0082

(a)

(b)

FIG. 2. (Color online) Comparison of numerically calculated nonlinear order parameter profiles u and v for {110} crystal faces obtained from the PFC amplitude equations (blue dashed line) and the GL theory (Ref. 44) (red solid line) and computed form MD simulations with $\vec{K}_{101}$ and $\vec{K}_{110}$ for u and v, respectively (solid circles).

As seen from Table II, the agreement between the different continuum theories and MD simulations is poorer for the ratio $\gamma_{111}/\gamma_{100}$ than for $\gamma_{110}/\gamma_{100}$. Consequently, the ϵ_1 and ϵ_2 values, which depend on these two ratios, are not well predicted by these theories in comparison to ϵ_4, which depends only on $\gamma_{100}/\gamma_{110}$. This discrepancy appears to be an intrinsic limitation of weakly nonlinear theories where anisotropy is computed using only one set of density waves associated with principal reciprocal lattice vectors of magnitude K_{max}. While this one-set approximation is reasonably good on the liquid side of the interface, where the density wave amplitude is small, it breaks down on the solid side where the highly nonlinear crystal density field is better approximated by sharply peaked Gaussians centered around atomic positions. Resolving this field requires a very large number of sets of reciprocal lattice vectors.[29]

An interesting related issue is the sensitivity of crystalline anisotropy to microscopic details of interatomic potentials.

MD simulations to date indicate that the magnitude of this anisotropy tends to be larger for fcc than bcc forming systems, suggesting that crystal structure is a main determinant of anisotropy. Despite this trend, anisotropy values do depend on the choice of potentials for a given crystal structure. For example, two other interatomic potentials for Fe yield values of ϵ_4 twice smaller than for the MH(SA)^2 potential.[9]

In contrast, anisotropy values are independent of material parameters in both the PFC amplitude equations and GL theory. The reason is that all the material-dependent input parameters, which include the density wave amplitude in the solid u_s and peak liquid structure factor properties, can be scaled out of the free-energy functionals for these theories. This is readily seen in the dimensionless form of the free-energy functional for the PFC amplitude equations given by Eq. (30). Consequently, the ratios of γ values for different crystal faces that determine the anisotropy parameters ϵ_1 and ϵ_2 are universal for all bcc elements within the confines of each theory, and the value of anisotropy parameters depend on the nonlinear coupling between density waves. The results of Table II show that differences in these couplings (i.e., coefficients of quartic terms in the free-energy functionals) lead to only small differences of anisotropy values. It is possible, however, that other choices could produce values of ϵ_1 and ϵ_2 in closer agreement with MD simulations.

VI. CONCLUSIONS

We have studied equilibrium properties of bcc-liquid interfaces in a physically motivated small ϵ limit of the PFC model,[19,20] where the freezing transition is weakly first order. This limit lends itself naturally to a multiscale analysis that was used to derive a set of equations for the leading order amplitudes A_i^0 of density waves corresponding to the set $\{\vec{K}_i\}$ of principal reciprocal lattice vectors, and to express the free-energy of the solid-liquid system as a functional of these amplitudes. Furthermore, by exploiting the close analogy between this functional and GL theory derived from classical DFT,[44,45] we have determined all the parameters of the PFC model in terms of peak properties of the liquid structure factor and the solid density wave amplitude.

In both the PFC amplitude equations and GL theory, the anisotropy of γ originates from the directional dependence (i.e., the dependence on $\vec{K}_i \cdot \hat{n}$ where $\hat{n}$ in the interface normal) of the coefficients of gradient-square terms ($|\vec{\nabla}A_i^0|^2$) in the free-energy functional, which govern the spatial decay rate of density waves in the liquid. In the isotropic limit where this directional dependence is neglected, and hence all amplitudes are equal, $A_i^0 = \phi$ for all i, both theories reduce to the conventional phase-field model of solidification formulated in terms of the nonconserved order parameter ϕ. From this standpoint, the present analysis relates formally the crystal and conventional phase-field models.

Numerical results show that the PFC model, the amplitude equations derived from this model, and GL theory[44] all give very similar predictions of γ and its anisotropy for parameters of Fe where ϵ is small enough ($\epsilon \approx 0.1$) for the amplitude equations to be quantitatively valid. The magnitude of γ, the shape of density wave profiles in the spatially

diffuse solid-liquid interface region, and the standard crystalline anisotropy parameter ϵ_4 defined in terms of the ratio $\gamma_{110}/\gamma_{100}$, are in good overall agreement with the results of MD simulations. The various continuum theories, however, do not predict accurately higher order anisotropies that also depend on the ratio $\gamma_{110}/\gamma_{100}$. These anisotropies probably depend generally on the contributions of higher sets of reciprocal lattice vectors, which are neglected in the simplest formulation of the PFC model considered here.

*Present address: Department of Materials Science and Engineering, Northwestern University, Evanston, IL 60208, USA.

[1] W. J. Boettinger, J. A. Warren, C. Beckermann, and A. Karma, Annu. Rev. Mater. Res. **32**, 163 (2002).

[2] L. Q. Chen, Annu. Rev. Mater. Res. **32**, 113 (2002).

[3] A. Karma, in *Handbook of Materials Modeling. Volume I: Methods and Models*, edited by S. Yip (Springer, Netherlands, 2005), pp. 2087–2103.

[4] J. S. Langer, in *Chance and Matter, Lectures on the Theory of Pattern Formation*, Les Houches, Session XLVI, edited by J. Souletie, J. Vannimenus, and R. Stora (North-Holland, Amsterdam, 1987), pp. 629–711.

[5] D. Kessler, J. Koplik, and H. Levine, Adv. Phys. **37**, 255 (1988).

[6] M. Ben Amar and E. Brener, Phys. Rev. Lett. **71**, 589 (1993).

[7] A. Karma and W. J. Rappel, Phys. Rev. Lett. **77**, 4050 (1996); Phys. Rev. E **57**, 4323 (1998).

[8] N. Provatas, N. Goldenfeld, and J. Dantzig, Phys. Rev. Lett. **80**, 3308 (1998).

[9] J. J. Hoyt, M. Asta, and A. Karma, Mater. Res. Soc. Symp. Proc. **41**, 121 (2003).

[10] T. Haxhimali, A. Karma, F. Gonzales, and M. Rappaz, Nat. Mater. **5**, 660 (2006).

[11] R. K. P. Zia and D. J. Wallace, Phys. Rev. B **31**, 1624 (1985).

[12] G. B. McFadden, A. A. Wheeler, R. J. Braun, S. R. Coriell, and R. F. Sekerka, Phys. Rev. E **48**, 2016 (1993).

[13] A. A. Wheeler and G. B. McFadden, Eur. J. Appl. Math. **7**, 367 (1996).

[14] J. M. Debierre, A. Karma, F. Celestini, and R. Guerin, Phys. Rev. E **68**, 041604 (2003).

[15] M. G. Day and A. Hellawell, Proc. R. Soc. London, Ser. A **305**, 473 (1968).

[16] R. E. Napolitano, H. Meco, and C. Yung, JOM **56**, 16 (2004).

[17] S. Henry, G.-U. Gruen, and M. Rappaz, Metall. Mater. Trans. A **35**, 2497 (2004).

[18] M. Rappaz, A. Jacot, and W. J. Boettinger, Metall. Mater. Trans. A **33**, 467 (2003).

[19] K. R. Elder, M. Katakowski, M. Haataja, and M. Grant, Phys. Rev. Lett. **88**, 245701 (2002).

[20] K. R. Elder and M. Grant, Phys. Rev. E **70**, 051605 (2004).

[21] K. R. Elder, N. Provatas, J. Berry, P. Stefanovic, and M. Grant, Phys. Rev. B **75**, 064107 (2007).

[22] P. M. Stefanovic, M. Haataja, and N. Provatas, Phys. Rev. Lett. **96**, 225504 (2006).

[23] J. Berry, M. Grant, and K. R. Elder, Phys. Rev. E **73**, 031609 (2006).

[24] G. H. Fredrickson and E. Helfand, J. Chem. Phys. **87**, 697 (1987).

[25] J. Swift and P. C. Hohenberg, Phys. Rev. A **15**, 319 (1977).

[26] M. C. Cross and P. C. Hohenberg, Rev. Mod. Phys. **65**, 851 (1993).

[27] T. V. Ramakrishnan and M. Yussouff, Phys. Rev. B **19**, 2775 (1979).

[28] A. D. J. Haymet and D. W. Oxtoby, J. Chem. Phys. **74**, 2559 (1981).

[29] B. B. Laird, J. D. McCoy, and A. D. J. Haymet, J. Chem. Phys. **87**, 5449 (1987).

[30] Y. Singh, Phys. Rep. **207**, 351 (1991).

[31] P. Harrowell and D. Oxtoby, J. Chem. Phys. **80**, 1639 (1984).

[32] Y. C. Shen and D. Oxtoby, J. Chem. Phys. **105**, 6517 (1996).

[33] Y. C. Shen and D. Oxtoby, J. Chem. Phys. **104**, 4233 (1996).

[34] J. Q. Broughton and G. H. Gilmer, J. Chem. Phys. **84**, 5759 (1986).

[35] R. L. Davidchack and B. B. Laird, Phys. Rev. Lett. **85**, 4751 (2000).

[36] R. L. Davidchack and B. B. Laird, J. Chem. Phys. **118**, 7651 (2003).

[37] R. L. Davidchack and B. B. Laird, Phys. Rev. Lett. **94**, 086102 (2005).

[38] J. J. Hoyt, M. Asta and A. Karma, Phys. Rev. Lett. **86**, 5530 (2001).

[39] J. R. Morris, Phys. Rev. B **66**, 144104 (2002).

[40] J. J. Hoyt and M. Asta, Phys. Rev. B **65**, 214106 (2002).

[41] D. Y. Sun, M. Asta, J. J. Hoyt, M. I. Mendelev, and D. J. Srolovitz, Phys. Rev. B **69**, 020102(R) (2004).

[42] D. Y. Sun, M. Asta, and J. J. Hoyt, Phys. Rev. B **69**, 174103 (2004).

[43] J. J. Hoyt, M. Asta, and D. Y. Sun, Philos. Mag. **86**, 3651 (2006).

[44] K.-A. Wu, A. Karma, J. J. Hoyt, and M. Asta, Phys. Rev. B **73**, 094101 (2006).

[45] W. H. Shih, Z. Q. Wang, X. C. Zeng, and D. Stroud, Phys. Rev. A **35**, 2611 (1987).

[46] A. C. Newel and J. A. Whitehead, J. Fluid Mech. **38**, 203 (1969).

[47] N. Goldenfeld, B. P. Athreya, and J. A. Dantzig, Phys. Rev. E **72**, 020601(R) (2005).

[48] B. P. Athreya, N. Goldenfeld, and J. A. Dantzig, Phys. Rev. E **74**, 011601 (2006).

[49] M. I. Mendelev, S. Han, D. J. Srolovitz, G. J. Ackland, D. Y. Sun, and M. Asta, Philos. Mag. **83**, 3977 (2003).